Journal of Materials Chemistry C

Accepted Manuscript

This article can be cited before page numbers have been issued, to do this please use: H. Zhang, J. Zeng, W. Luo, H. Wu, C. Zeng, K. Zhang, W. Feng, Z. Wang, Z. Zhao and B. Z. Tang, *J. Mater. Chem. C*, 2019, DOI: 10.1039/C9TC01453E.

ROYAL SOCIETY OF CHEMISTRY

rsc.li/materials-c

View Article Online
DOI: 10.1039/C9TC01453E

ARTICLE

Synergistic Tunings on Optical and Electrical Performance of AIEgens with Hybridized Local and Charge-Transfer Excited State

Received 00th January 20xx,
Accepted 00th January 20xx

DOI: 10.1039/x0xx00000x

Han Zhang,[a] Jiajie Zeng,[a] Wenwen Luo,[a] Haozhong Wu,[a] Cheng Zeng,[a] Kexin Zhang,[a] Weiqiang Feng,[a] Zhiming Wang,*[,a,c] Zujin Zhao*[,a] and Ben Zhong Tang*[,a,b]

The reported organic light-emitting diodes (OLEDs) based on hybridized local and charge-transfer (HLCT) state emitters mostly exhibt low photoluminescence quantum yields (PLQYs) in aggregates, failing to achieve the best device efficiency although they exhibit good exciton utilization efficiencies (EUEs). In this work, by introducing aggregation-induced emission (AIE) moiety (tetraphenylethene, TPE) and cyano group (CN) to HLCT-typed core, phenanthroimidazole (PI), six luminescent compounds with different conjugation patterns at C2 and N1 substituent positions are obtained, and their excited states are regulated effectively. Based on systematic photophysical analysis, the impacts of molecular conjugation patterns on regulation of the locally excited (LE) and charge-transfer (CT) component are disclosed, and their AIE characters that ensure high PLQYs of these compounds in aggregates are observed. Exciton conversion channels from triplets to singlets via excited states tunings are proposed based on theoretical calculations. The non-doped OLEDs based on these compounds exhibit excellent performances with maximum luminance, current efficiency, and external quantum efficiency of up to 31070 cd m^{-2}, 18.46 cd A^{-1}, and 7.16 %, respectively, and very small efficiency roll-off of 4.0 % at 1000 cd m^{-2} luminance. The successful design in these HLCT-based AIEgens not only gives more optimization choices for OLED emitters, but also proves that a strategy of reasonably superposing AIE unit to HLCT emitters is feasible in materials design.

Introduction

Organic light-emitting diodes (OLEDs) have been extensively developed for the practical applications in flat-panel display and solid-state lighting technologies owing to various superior features such as low energy cost, high brightness, high-quality color, light weight, and flexibility, etc.[1] To achieve high electroluminescence (EL) efficiencies, two main factors of the luminescent materials, photoluminescence quantum yields (PLQY) in solid state and exciton utilization efficiency (EUE), play crucial roles in the working process, which deserve particular attentions in materials design. In fact, the EUEs of most traditional fluorescent emitters are theoreticallly limited to 25% (a maximum) from electro-generated singlet excitons according to the spin statistics,[2] but a greater proportion of triplet excitons (75%) are failed to generate photons and lost by means of non-radiative decay because of spin forbidden from triplet to singlet. Therefore, harvesting triplet excitons for light emission has been recoganized an effective strategy to increase EL efficiencies in OLEDs.

Currently, thermally activated delayed fluorescence (TADF),[3] triplet-triplet annihilation (TTA)[4] and hybridized local and charge-transfer (HLCT) state[5] mechanisms are developed to solve the problem of triplet exciton utilization in pure organic emitters. Actually, considerable successes have been achieved based on these mechanisms, leading to greatly boosted EL efficiencies of noble-metal free ognaic emitters. Among them, HLCT mechanism has drawn increasing attention in recent years because it is conducive to both PLQY and EUE.[6] In HLCT emitters (Fig. 1A), the dominant locally excited (LE) in the hybridized state at low-lying S_1 is liable to fluoresce intensely due to a large overlap between hole and electron wave functions, and generates a large singlet–triplet energy splitting between S_1 and T_1 (ΔE_{S1T1}); while at high-lying levels, the charge transfer (CT) component in hybridized state leads to activating the "hot exciton" channels with a negligible ΔE_{SmTn} (m≥1, n≥2), enabling reverse intersystem crossing (RISC) process and thus increasing EUE.[6d] The EUEs of many reported HLCT emitters are close to 100 %, but their PLQYs are not high enough in neat films in practice due to aggregation-caused quenching (ACQ) phenomenon, which undermines their EL performance.[5d,6c] In addition, seeking for molecular design strategies and excited state modulation principles for HLCT emitters is still a challenging task.

Recently, aggregation-induced emission (AIE) offers high possibility to solve the ACQ problem of most traditional chromophores,[7] and the luminogens with AIE characteristics (AIEgens)[8] can fluoresce intensively when they are fabricated into neat films, which are considered as ideal light-emitting materials for

[a] SCUT-HKUST Joint Research Institute, Guangzhou International Campus, Center for Aggregation-Induced Emission, State Key Laboratory of Luminescent Materials and Devices, South China University of Technology, Guangzhou 510640, China.
*E-mail: wangzhiming@scut.edu.cn; mszjzhao@scut.edu.cn
[b] Department of Chemistry, Hong Kong Branch of Chinese National Engineering Research Center for Tissue Restoration and Reconstruction, The Hong Kong University of Science and Technology, Clear Water Bay, Kowloon, Hong Kong, China. *E-mail: tangbenz@ust.hk
[c] School of Petrochemical Engineering, Shenyang University of Technology, Liaoyang 111003, China.

†Electronic Supplementary Information (ESI) available: Experimental details, X-ray crystallography, device fabrication, TGA curves and DSC spectra, PL spectra in THF, additional AIE curves, time-resolved fluorescence decay curves in THF solutions and neat films, detailed theoretical calculations data, mechanochromism properties measurement and ^{1}H and ^{13}C NMR spectra. See DOI: 10.1039/x0xx00000x

View Article Online
DOI: 10.1039/C9TC01453E

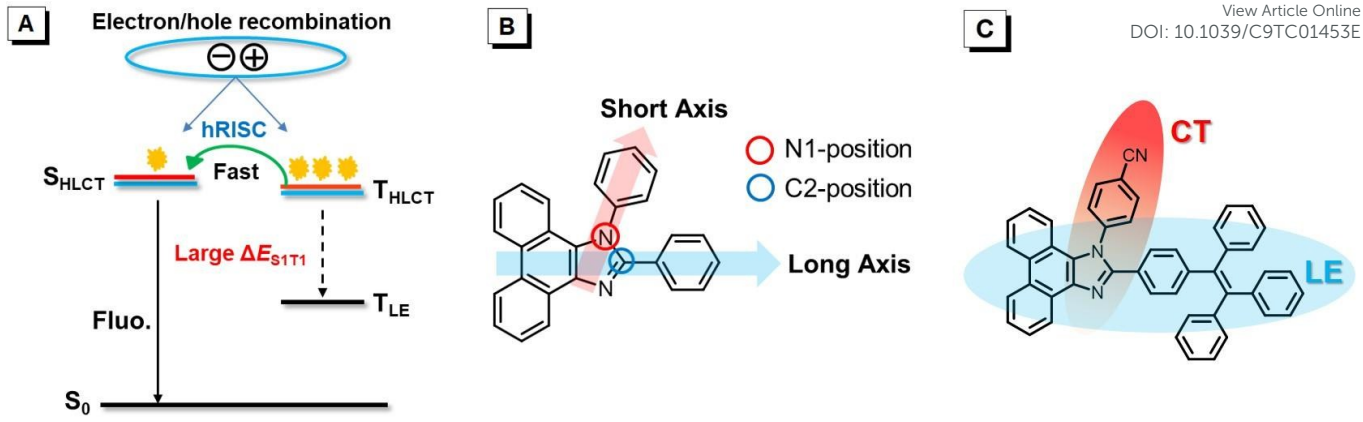

Fig. 1 (A) Typical energy level character of HLCT emitter with "hot exciton" channel; (B) The long-short axis design based on phenanthroimidazole in this work. (C) Construction of LE state and CT state in the PI derivative (taking *pp*CTPI as an example).

non-doped OLEDs.[9] Hence, it is a promising strategy to achieve a win-win situation via combining HLCT process with AIE nature.[10] Herein, we chose a typical HLCT unit, phenanthroimidazole (PI), to function as an emissive core in molecular design (Fig. 1B and 1C).[11] And a star AIE molecule, TPE, is introduced into the C2-position of imidazole ring in PI (defined as the long axis in molecular structure) with different patterns (*para*- and *meta*- linkages). Thereby, we can tune the LE component in hybridized excited states and luminescence behaviors in the aggregated states via different conjugated degrees. At the N1-position (defined as the short axis in molecular structure), a benzonitrile with cyano group (CN) at *meta*- or *para*- pattern was inserted to tune the CT component in HLCT state. Then, six AIEgens, *p*TPI,[12a] *mp*CTPI, *pp*CTPI, *m*TPI, *mm*CTPI and *pm*CTPI, were synthesized and characterized (Fig. 2). The substituent effects on their photophysical and electrochemical properties of the six compounds were systematically investigated. They showed prominent AIE characteristics and high PLQYs in aggregates. Their EUEs can be enhanced by tuning excited state to promote exciton conversion channels based on theoretical calculations, which was confirmed in subsequent EL performances. The non-doped OLED using *pp*CTPI as an emitter exhibited the best EL performance with excellent external quantum efficiency (7.16%, EQE) and EUEs (>48%), and their maximum luminance, current efficiency, and power efficiency (L, η_c, and η_p) are of up to 31070 cd m^{-2}, 18.46 cd A^{-1} and 16.32 lm W^{-1}, respectively. In addition, ultra-low roll-off of 4.0% at 1000 cd m^{-2} luminance was observed. These results demonstrated a feasible strategy of tuning excited state distributions by reasonably combining HLCT materials with AIE nature for the development of high-efficiency emitters for OLEDs.

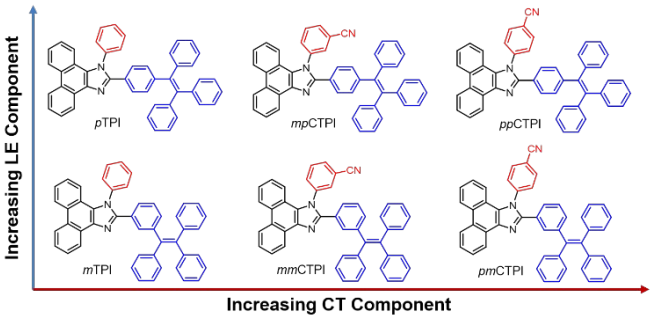

Fig. 2 Chemical structures of the six PI derivatives.

Results and discussion

Synthesis and crystal structure

Phenanthrenequinone, the corresponding aromatic amines, aromatic aldehydes and ammonium acetate were chosen to obtain the target compounds via a one-pot reaction in good yields. The detailed synthetic routes, preparation methods and characterization data of these final products are described in the Supporting Information (Fig. S1†). Single crystals of *m*TPI were grown from the ethanol and dichloromethane mixture by slow solvent diffusion and evaporation. As depicted in Fig. 3, a twisted conformation with a big dihedral angel of 78.51° and a planar conformation with a small dihedral angel of 33.59° are observed at N1-position and C2-position

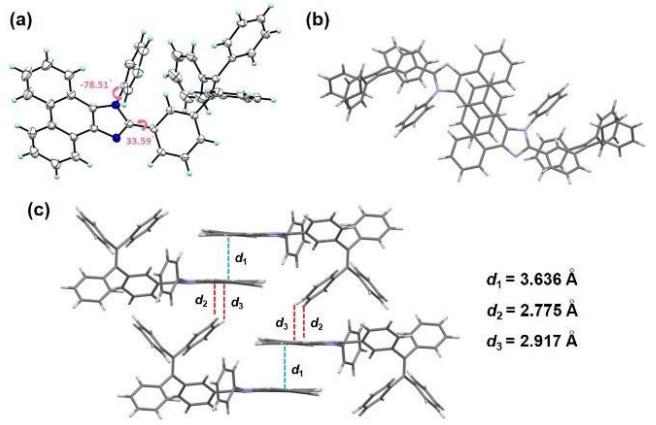

Fig. 3 (a) ORTEP drawing of the crystal structure (CCDC 1903655) of *m*TPI and (b, c) packing pattern of *m*TPI in crystal.

View Article Online
DOI: 10.1039/C9TC01453E

Table 1 Photophysical and thermal properties of the compounds. [a]

	λ_{abs} (nm)	λ_{em} (nm)			Φ_F (%)			α_{AIE}	τ (ns) [k_r (ns^{-1}), k_{nr} (ns^{-1})]		T_g/T_d (°C)
		soln	aggr	film	soln	aggr	film		soln	film	
*p*TPI	365	432,465	483	493	0.3	69.4	88.5	231.3	0.73 (0.004, 1.366)	2.63 (0.337, 0.044)	nd/389
*mp*CTPI	361	433,461	485	503	0.5	64.2	67.2	128.4	0.84 (0.006, 1.185)	2.37 (0.284, 0.138)	nd/443
*pp*CTPI	361	433,460	475	501	0.5	61.2	59.5	122.4	1.06 (0.005, 0.939)	2.85 (0.209, 0.142)	nd/415
*m*TPI	362	389,410	465	491	0.5	39.4	47.6	78.8	1.03 (0.005, 0,966)	4.19 (0.114, 0.125)	114/402
*mm*CTPI	359	389,412	464	493	0.6	33.5	23.8	55.8	1.94 (0.003, 0.512)	3.97 (0.060, 0.192)	126/408
*pm*CTPI	359	423	467	492	1.2	31.3	20.5	26.1	1.14 (0.011, 0.867)	4.26 (0.048, 0.187)	128/414

[a] soln = THF solution (10^{-5} M); aggr = nanoaggregate formed in H_2O/THF mixture with a f_w of 90%; film = vacuum-deposited neat film; Φ_F = absolute PL quantum yield determined by a calibrated integrating sphere; α_{AIE} = value of AIE effect, calculated by Φ_F (aggr)/Φ_F (soln); τ = PL lifetimes measured at room temperature in air; k_r = radiative decay rate ($k_r = \Phi_F/\tau$); k_{nr} = nonradiative decay rate ($k_{nr} = (1 - \Phi_F/\tau)$); nd = not detectable.

of *m*TPI, respectively. The molecular packing of *m*TPI shows an antiparallel arrangement, in which TPE and PI units form a head-to-tail stacking. As a result, the twisted TPE unit can interrupt the π-π stacking interactions among PI units with interplane distance of 3.636 Å. The distances of 2.775 Å and 2.917 Å between the hydrogen atoms of the TPE phenyl rings and the π-electrons of PI indicate C–H···π hydrogen-bond interactions existed in crystals, which can restrict and lock the molecular rotations of TPE and lead to reduction of the non-radiative energy loss via rotational relaxation.

Thermal properties

The thermal properties of the six compounds were examined using thermogravimetric analysis (TGA) and differential scanning calorimetry (DSC) methods under N_2 atmosphere. As shown in Fig. S2† and Table 1, all the compounds exhibited high thermal decomposition temperatures (T_d, corresponding to 5% weight loss) in the range of 389–443 °C. While, the four cyano-containing compounds had better thermal stabilities, like our previous findings.[11a] DSC measurements were carried out from 30 °C to 360 °C, and the three TPE *meta*-linked compounds, *m*TPI, *mm*CTPI and *pm*CTPI, revealed distinct glass transition temperatures (T_g) of 114 °C, 126 °C and 128 °C, respectively. No obvious T_g peaks could be detected in their counterparts, but crystallization temperatures (T_c) of 202 °C for *p*TPI and 210 °C for *mp*CTPI were observed. These results indicated the good thermal and morphological stabilities of the six compounds, which would have positive effects on the performance of their OLED devices.

Photophysical properties

Fig. 4A shows the ultraviolet-visible (UV-vis) absorption spectra of the compounds in tetrahydrofuran (THF, [c] = 1×10^{-5} M). The sharp absorptions at 260 nm in all compounds were considered as typical π-electron response of the phenanthrene derivative.[11b] The long-wavelength absorption bands at 300–370 nm might be attributed to the π–π* transitions at the long-axis direction.[11b,13] Red-shifted and enhanced absorption bands were found in TPE *para*-linked compounds because of their more effective conjugation than TPE *meta*-linked ones. Interestingly, there was negligible change in absorption spectra before and after cyano group introduction, which indicated that ICT effect along N1-substitution direction had little influence on absorption process and optical band gaps of the compounds.

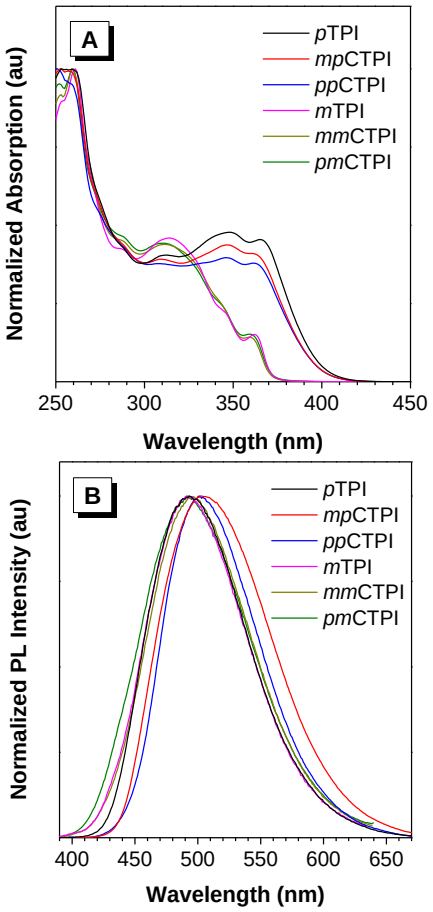

Fig. 4 (A) Absorption spectra in THF solutions (10^{-5} M) and (B) PL spectra in neat films of the compounds.

The photoluminescence (PL) spectra of these compounds in dilute THF solutions (10^{-5} M) and neat films were displayed in Fig. S3† and Fig. 4B. In THF solutions, three TPE *para*-linked compounds exhibited blue emissions ranging from 409–487 nm with hyperfine vibrational structures in their PL spectra, indicating LE components were dominant in their HLCT states according to the previous reports about PI-based deactivates.[5a,12a] When the linkage of TPE unit was changed into *meta*-linked form, their conjugation degree at long-axis direction was decreased, resulting in bluer emissions and less LE components. However, their hyperfine vibrational structure vanished gradually after cyano group insertion, and the emission was red-shifted at the same time, implying increased CT proportion at short-axis direction. In the vacuum-deposited neat films, *p*TPI, *mp*CTPI and *pp*CTPI showed broad PL peaks at 493, 503 and 501 nm, respectively, and the other three ones emitted sky-blue PL ranging from 491–493 nm. In comparison with those in solutions, the emission peaks in films are much red-shifted. This is because the molecule packing in film can decrease the degree of twisting of TPE unit, and thus prolong the conjugation length and give rise to a large redshift. All compounds were weakly fluorescent with low absolute PL quantum yields (Φ_F) of 0.3–1.2 % in THF solutions, but emitted intensely in neat films, demonstrating notable AIE nature. The Φ_Fs of TPE *para*-linked compounds in neat films were higher than those of their counterparts because of enlarged degree of effective π-conjugation at long-axis, and *p*TPI had a highest value of 88.5%. As the addition of cyano group, the Φ_Fs of the emitters were decreased, indicating the increment of CT-component had negative effect on their luminescence efficiencies. It was worth noting that the six compounds exhibited mechanochromism properties.[12a] The PL emissions of neat films were closer to the ones from ground states (see ESI), indicating the fromation of amorphous states in vacuum deposition films. Their absolute Φ_Fs in different states were listed in Table 1. Solvatochromic experiments of PL were employed to exam complex HLCT changes in composition.[5a,14] However, the emissions in some high-polar solvents were too weak to detect accurately because of their faint fluorescence caused by their AIE nature. Therefore, the tuning processes of LE and CT distribution and proportion were confirmed by theoretical calculation instead.

For investigating their AIE characteristics, water, a poor solvent of the compounds, was added into their THF solutions in different proportions (Fig. 5 and Fig. S4†). The emissions of the six compounds were very weak in a low water fraction (f_w), but became stronger as the increment of f_w. Consequently, their Φ_Fs got dozens and even hundreds of times enhancement in aqueous condition. The greatly

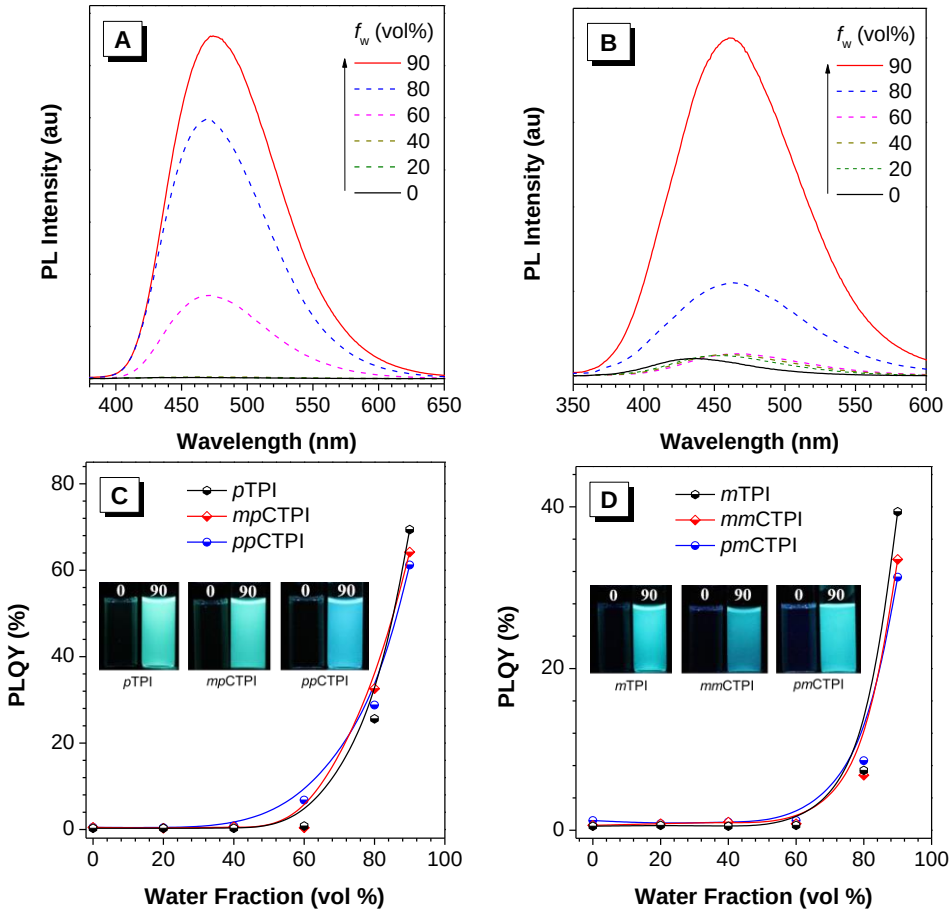

Fig. 5 PL spectra of (A) *pp*CTPI, (B) *pm*CTPI in THF/water mixtures (10^{-5} M) with different water fractions (f_w); (C) and (D) PLQY versus f_w curves; Inset: photos of the compounds in THF/water mixtures (f_w = 0 and 90%), taken under 365 nm excitation.

View Article Online
DOI: 10.1039/C9TC01453E

enhanced PL efficiencies should be attributed to the restriction of rotational motions by the spatial constraint in the aggregated state and thus the suppression of nonradiative decay of the excited state.[15] To further understand the relevant photophysical process, the transient fluorescence spectra were measured (Fig. S5†). As listed in Table 1, all the compounds showed longer fluorescence lifetimes in neat films than in THF solutions. Their non-radiative decay rates (k_{nr}) were decreased greatly from solutions to films, which enabled them to emit more efficiently in aggregates with obvious PLQYs improvement. The compounds showed single index decay of lifetime without delayed component, which confirmed that there were no TADF or TTA mechanisms in luminescence process of these compounds.[16]

Table 2 Electrochemical data of the compounds. [a]

	E^{ox}_{onset} (V)	E^{red}_{onset} (V)	HOMO (eV)	LUMO (eV)	E_g^e (eV)	E_g^o (eV)
*p*TPI	0.92	–2.29	–5.49	–2.44	3.05	3.13
*mp*CTPI	0.97	–2.20	–5.54	–2.53	3.01	3.14
*pp*CTPI	0.97	–2.19	–5.55	–2.54	3.01	3.14
*m*TPI	0.99	–2.38	–5.56	–2.34	3.22	3.34
*mm*CTPI	1.06	–2.22	–5.63	–2.51	3.12	3.34
*pm*CTPI	1.07	–2.24	–5.64	–2.50	3.13	3.34

[a] E^{ox}_{onset}: onset oxidation potential; E^{red}_{onset}: onset reduction potential; E_g^e = LUMO – HOMO; $E_g^o = 1240/\lambda$, λ gained from absorption spectra.

Electrochemical properties and theoretical calculations

The CV measurements were conducted in CH_2Cl_2 for oxidation potentials and DMF for reduction potentials using 0.1 M tetra-*n*-butylammonium-hexafluoro-phosphate (*n*-Bu_4NPF_6) as the electrolyte. The HOMO and LUMO energy levels were determined using ferrocene (Fc) as the reference (4.8 eV) and were calibrated with respect to $E_{1/2}$ (Fc/Fc^+) in every measurement.[17] Their cyclic voltammograms were given in Fig. S6† and the corresponding data were summarized in Table 2. The HOMO energy levels of *p*TPI, *mp*CTPI, *pp*CTPI, *m*TPI, *mm*CTPI and *pm*CTPI were calculated to be –5.49, –5.54, –5.55, –5.56, –5.63, and –5.64 eV, respectively, which were similar to those of reported PI-based derivatives.[11] The LUMO energy levels of *p*TPI and *m*TPI were estimated to be –2.44 eV and –2.34 eV, and probably populated on the TPE (as an acceptor compared to PI). The other four compounds with cyano group had lower LUMO energy levels of –2.53, –2.54, –2.51, and –2.50 eV, respectively, indicating that the distribution of LUMOs had changed. For further comparison, the electrical bandgaps (E_g^e) of the compounds became narrower after cyano group insertion, quite different from their optical bandgaps (E_g^o) discussed in absorption spectra. Such measurement results indicated that there might be separations of electrical and optical energy gaps character in cyano-containing compounds, which could be beneficial to constructing lower injection/transport barrier in wide-band gap luminescent materials.[18]

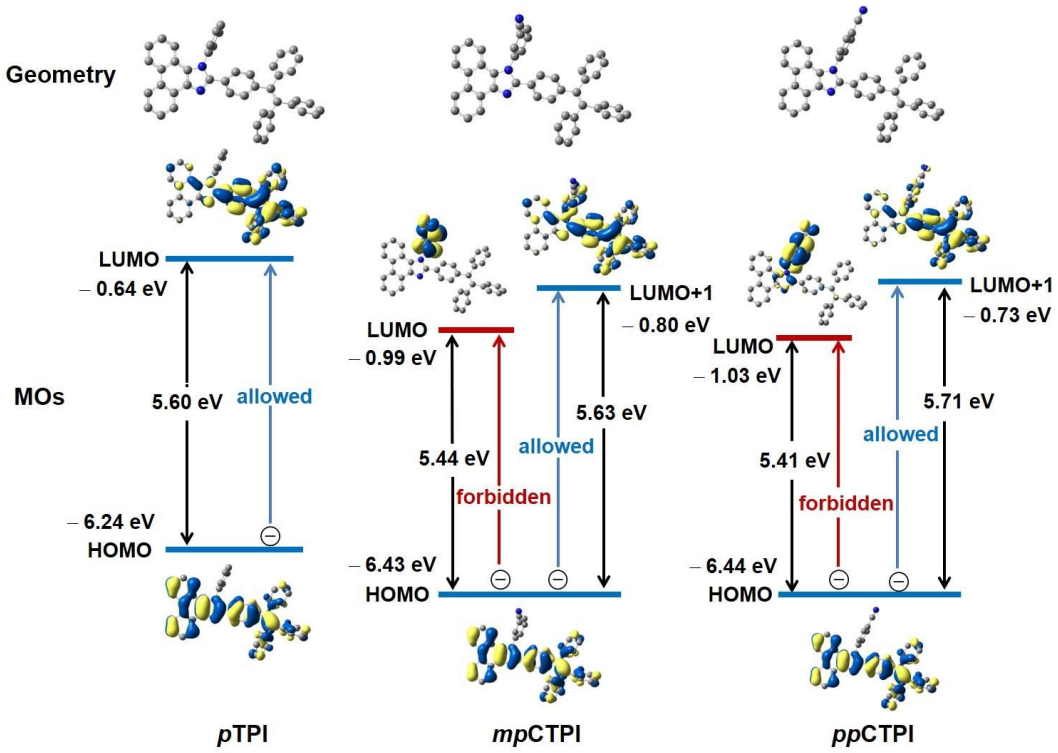

Fig. 6 Relevant molecular orbital amplitude plots, energy levels and possible transition sketch maps of TPE *para*-linked compounds.

View Article Online
DOI: 10.1039/C9TC01453E

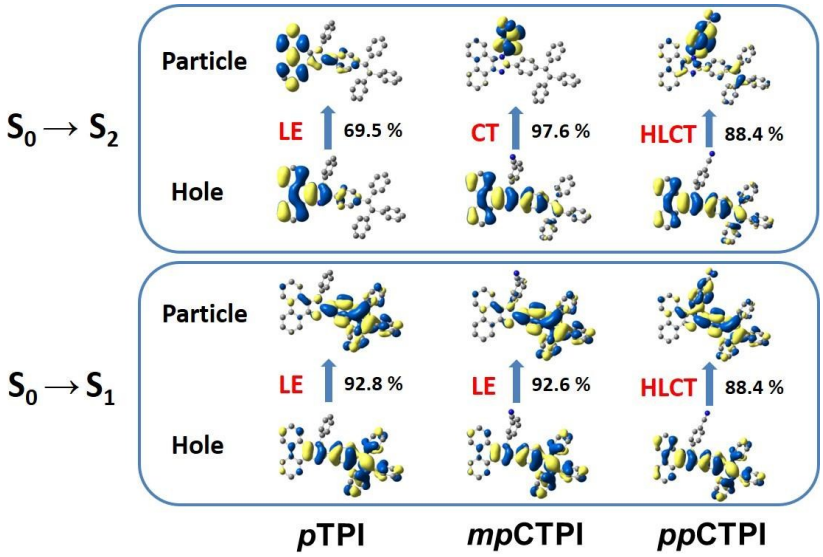

Fig. 7 Natural transition orbitals and properties of $S_0 \rightarrow S_1$ and $S_0 \rightarrow S_2$ for *p*TPI, *mp*CTPI and *pp*CTPI, calculated by M06-2X hybrid functional at the basis set level of 6-31G (d, p).

To further understand their different energy gaps obtained from absorption spectra and CV measuements, the density functional theory (DFT) calculations were carried out at level of M0-62X/6-31G(d,p) employing the Gaussian 09 package. The geometries, molecular orbitals (MOs) and calculated energy levels were shown in Fig. 6 and Fig. S7†. The HOMOs of the compounds were mainly located on the PI unit and TPE moiety at long-axis direction, and little decrements were observed in their calculated HOMO values after cyano group was inserted. The LUMOs of both *m*TPI and *p*TPI were mostly populated on TPE acceptor, which well agreed with the analysis above. After inserting cyano group, the distribution of LUMOs was transferred into N1-imidazole position owing to their enhanced electron-withdrawing abilities,[11c] and these lower LUMO values of cyano-containing compounds were agreed to the results in electrochemical measurements. Interestingly, the LUMO+1 levels of compounds with cyano group located mostly in TPE unit, similar to their respective matrix situations (LUMOs in *m*TPI and *p*TPI). Their caculated energy gaps from HOMO to LUMO+1 were 5.63 eV for *mp*CTPI, 5.71 eV for *pp*CTPI, 5.94 eV for *mm*CTPI, and 5.97 eV for *pm*CTPI, respectively, and these values were close to energy gaps from HOMO to LUMO in *p*TPI and *m*TPI (5.60 eV and 5.91 eV), respectively. Exactly, these resluts were consitent with optical bandgaps gained from absorption spectra. Now, the hypothesis of separation of electrical and optical energy gaps was confirmed. In fact, the transitions from HOMO to LUMO in non-cyano-containing compounds and from HOMO to LUMO+1 in cyano-containing compounds were allowed because of their effective overlaps in the MOs. However, the transitions from HOMO to LUMO in the latter were nearly forbidden in photo-absorption process, owing to the complete separation characters. Wherein, the large twisting dihedral angles between N1-phenyl and PI plane (78° for *p*TPI, 77° for *mp*CTPI, 75° for *pp*CTPI, 80° for *m*TPI, 77° for *mm*CTPI and 76° for *pm*CTPI) gave considerable contributions to the separation of the MOs.[19]

Excited States Properties

In order to examine the excited states properties of the compunds, natural transition orbitals (NTOs) for the $S_0 \rightarrow S_n$ and T_n (n = 1–8) transition were performed using time-dependent density functional theory (TD-DFT) method (Table S2-7 and Fig. S8†).[20] As shown in Fig. 7, for the $S_0 \rightarrow S_1$ transition in *p*TPI, the "hole" and "particle" were mostly located on imidazole ring and TPE moiety. This distribution was assigned to LE transition, and the large overlap of the NTO in TPE implied the compouds would have high fluorescence efficiency and AIE characteristic.[12a] A homologous LE character on PI moiety was also observed in $S_0 \rightarrow S_2$ transition. Along with the introduction of cynao group into N1-phenyl, the ICT process was activitaed and the distribution of NTOs became more complicated. In *mp*CTPI, the $S_0 \rightarrow S_1$ transition exhibited nearly the same LE configuration with *p*TPI, but the distinct CT transition with the "hole" in PI and "particle" in N_1-CN-phenyl could be found in $S_0 \rightarrow S_2$ transition, implying the high-energy CT state was constructed in its excited states as our expected. When the cyano group was linked at the *para*-position, the increased electron-withdrawing ability at the short axis direction generated a larger CT component in *pp*CTPI, which could contribute to $S_0 \rightarrow S_1$. The"hole" and "particle" NTOs for S_1 and S_2, taking on partial separation and partial overlap, were considered as class HLCT states.[5d,6b] Similar situation arose in TPE *meta*-linked compounds (Fig. S9†), wherein, *mm*CTPI and *pm*CTPI contained better mixed LE/CT component than *m*TPI as well. However, the higher CT components in *mm*CTPI and *pm*CTPI were observed because of the lower conjugation degree caused by TPE *meta*-linked pattern. Importantly, the

View Article Online
DOI: 10.1039/C9TC01457F

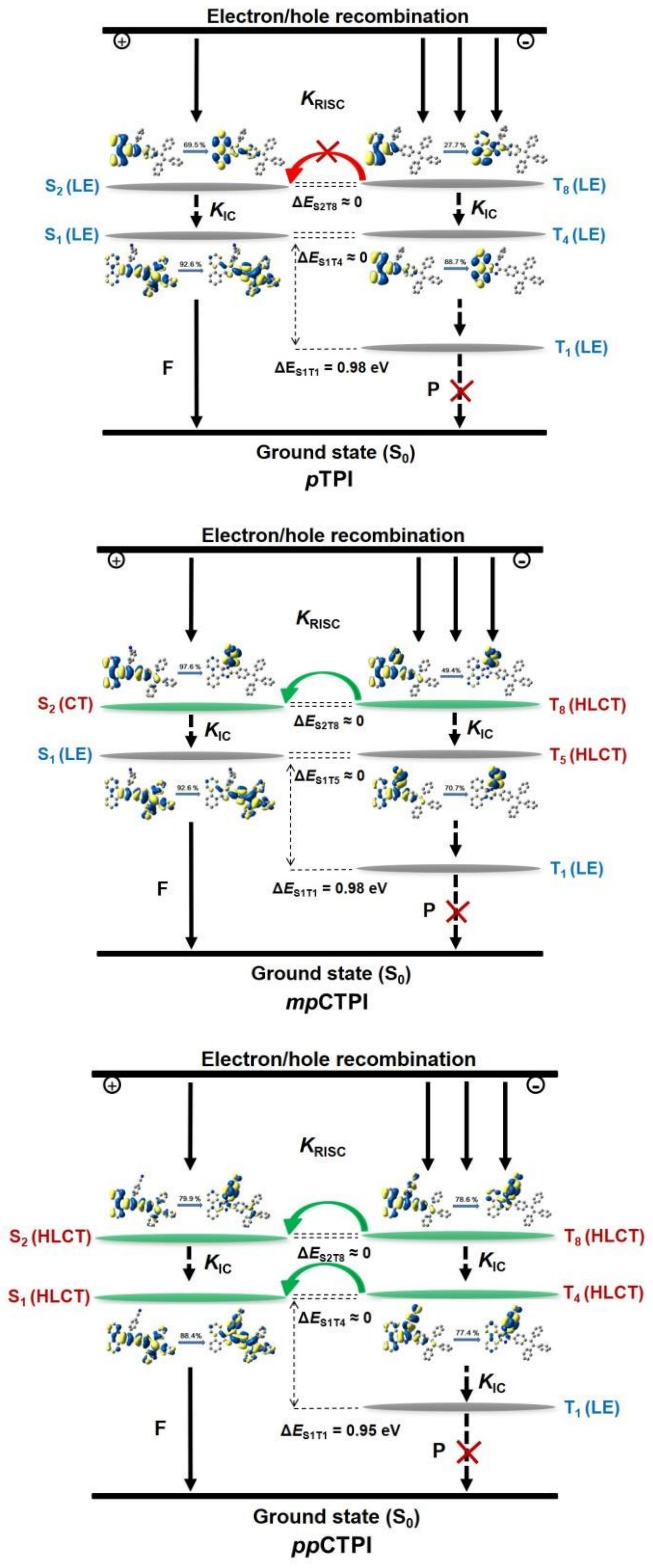

Fig. 8 Probable "hot exciton" mechaniam caused by HLCT states for TPE *para*-linked compounds. Here, S: singlet state; T: triplet state; LE: local excited-state; CT: charge-transfer state; ΔE_{ST}: singlet–triplet energy splitting; K_{IC}: internal conversion rate; K_{RISC}: reverse intersystem crossing rate.

oscillator strength of $S_0 \rightarrow S_1$ ($f_{S0\text{-}S1}$) that was considered to be related to the PLQYs of emitters was reduced as the addition of cyano group, with values of 0.9570 for *p*TPI, 0.9490 for *mp*CTPI and 0.8102 for *pp*CTPI, respectively (In counterparts, 0.3324 for *m*TPI, 0.2711 for *mm*CTPI and 0.0642 for *pm*CTPI). These obvious decreases in oscillator strength were in good agreement with the PLQYs in experimental measurements (Table 1).

Compared with the common materials based on D–A or D–π–A system, this two-dimensional vertical conformation based long-short axis had a larger regulation space for CT proportion. The lowest luminous state remianed LE-like characters when the cyano group was inserted to N1-position at the short-axis, and there was only increment of the CT-component proportion in every excited state energy level. The feature had been mentioned in our previous reports: at the long axis of the emitter, the LE-dominated emissive state based on large π–conjugated structure needed to be constructed; and at its vertical direction, a short axis with obvious CT characteristic was built with large steric hindrance (the conjugation degree was not too large, or this short axis would become the emission axis).[6c,11] Hence, tunable CT-components could be incorporated into LE emissive state to form HLCT state. Combining AIE characteristics in further, the PLQYs in solid-state would be enhanced synchronously.

Why was the CT state required in the process of luminescence? In fact, the CT component does have negative effect on PLQYs, but it is liable to increase EUEs via RISC channels.[3a,5a,6c] For the "hot exciton" based on HLCT mechanism,
the complete conversion of excitons from triplet to singlet must meet three requirements in EL process: small ΔE_{SmTn} (m≥1, n≥2), CT component with weak exciton binding energy and obstacle for exciton relaxation from T_n to T_1.[6d,21] Wherein, the CT-typed exciton ususally have lower binding energy, and its generation is easier than LE-typed exciton after carrier injection and recombination, differnent from PL process. In other words, the formation of T_4 (CT-dominant) for *pp*CTPI was esaier than T_1 (LE-dominant) in OLEDs, and excitons might be converted into singlet from T_4 if there was a fast conversion channle. So, intrinsically, the appropriate proportion of CT component was very important to enhance the EUEs. By comparing all the detailed results of the excited states (Table S8-S13†), some valuable tendencies were observed. In *p*TPI and *m*TPI, every excitation in eight NTOs for triplet states mainly exhibited LE characters, as a result of noneffective RISC path to S_1 or S_2 ($T_{LE} \rightarrow S_{LE}$). For the high-lying S_2 and T_8 in *mp*CTPI, we found their ΔE_{ST} was very close with value of 0.05 eV and they both showed obvious CT character from NTOs, so the triplet excitons might be converted to singlet excitons *via* the RISC channel ($T_{HLCT} \rightarrow S_{CT}$). As the CT component became larger in other three cyano-containing compounds, the NTOs of both S_1 and S_2 took on HLCT character and more CT channels, such as S_1 and T_4 ($T_{HLCT} \rightarrow S_{HLCT}$), S_2 and T_8 ($T_{HLCT} \rightarrow S_{HLCT}$), could be found and generated more singlet excitons by more effective exciton up-conversion channels as shown in Fig. 8 and Fig. S10†. It was worth noting that the existence of several lower triplets (like T_2

View Article Online
DOI: 10.1039/C9TC01457F

and T_3 in *pp*CTPI) were unfavorable to RISC process and thus might make loss of harvesting triplet excitons.

EL performances

If the discussions above were correct, the gradual increment of EUEs could be expected in OLED performance. To evaluate their EL properties, we fabricated non-doped OLEDs with a device configuration of ITO/HATCN (5 nm)/TAPC (40 nm)/TCTA (5 nm)/ emitters (20 nm)/TmPyPB (40 nm)/LiF (1 nm)/Al (120 nm) (emiters = *p*TPI, device **I**; *mp*CTPI, device **II**; *pp*CTPI, device **III**; *m*TPI, device **IV**; *mm*CTPI, device **V**; *pm*CTPI, device **VI**), where HATCN (dipyrazino[2,3-*f*:2′,3′-*h*]quinoxaline-2,3,6,7,10,11-hexacarbo-nitrile) and LiF served as hole- and electro-injection layers, respectively; TAPC (di-(4-(N,N-ditolyl-amino)-phenyl)cyclohexan) and TmPyPB(1,3,5-Tri(m-pyridin-3-ylphenyl)benzene) worked as the hole- and electron-transporting layers, respectively; 4,4′,4′′-tris(carbazol-9-yl)-triphenylamine (TCTA) was used as the exciton blocking layer, and ITO (indium tin oxide) and Al were used as the anode and electrode, respectively. The schematic energy level diagrams of the devices, the EL spectra at 10 mA cm^{-2}, the current density–voltage–luminance (*J*–*V*–*L*) characteristics, the EQE *versus* luminance curves and the current efficiency *versus* luminance curves of the non-doped OLEDs were displayed in Fig. 9. The key data of device performances were summarized in Table 3, in which EUE was calculated by Eqn-1:

$$\eta_{EL} = \eta_{rec} \times \eta_s \times \eta_{PL} \times \eta_{out} \quad \text{(Eqn-1)}$$

Table 3 EL performances of the OLEDs based on the compounds.

Compounds	Device	λ_{EL} (nm)	V_{on} (V)[a]	L (cd m^{-2})[b]	η_c (cd A^{-1})[b]	η_p (lm W^{-1})[b]	CIE (x, y)[c]	EUE (%)	EQE_{max} (%)[b]	EQE_{100} (%)	RO (%)
*p*TPI	I	494	2.9	40290	16.52	15.55	(0.226, 0.423)	28.6	6.32	6.07	4.0
*mp*CTPI	II	506	2.9	36030	18.27	19.12	(0.243, 0.447)	39.9	6.71	6.26	6.7
*pp*CTPI	III	503	3.1	31070	18.46	16.32	(0.211, 0.402)	48.1	7.16	6.83	4.6
*m*TPI	IV	492	3.1	12310	8.87	8.70	(0.201, 0.339)	33.4	3.98	3.23	18.8
*mm*TPI	V	493	3.5	5386	5.07	3.93	(0.213, 0.345)	38.2	2.27	2.14	5.7
*pm*TPI	VI	489	2.9	6748	5.44	5.34	(0.195, 0.342)	48.4	2.48	2.04	17.7

[a] V_{on} is the turn-on voltage at 1 cd m^{-2}. [b] The luminescence (L), current efficiency (η_c), power efficiency (η_p) are the maximum values of the devices. [c] CIE coordinates at 10 mA cm^{-2}.

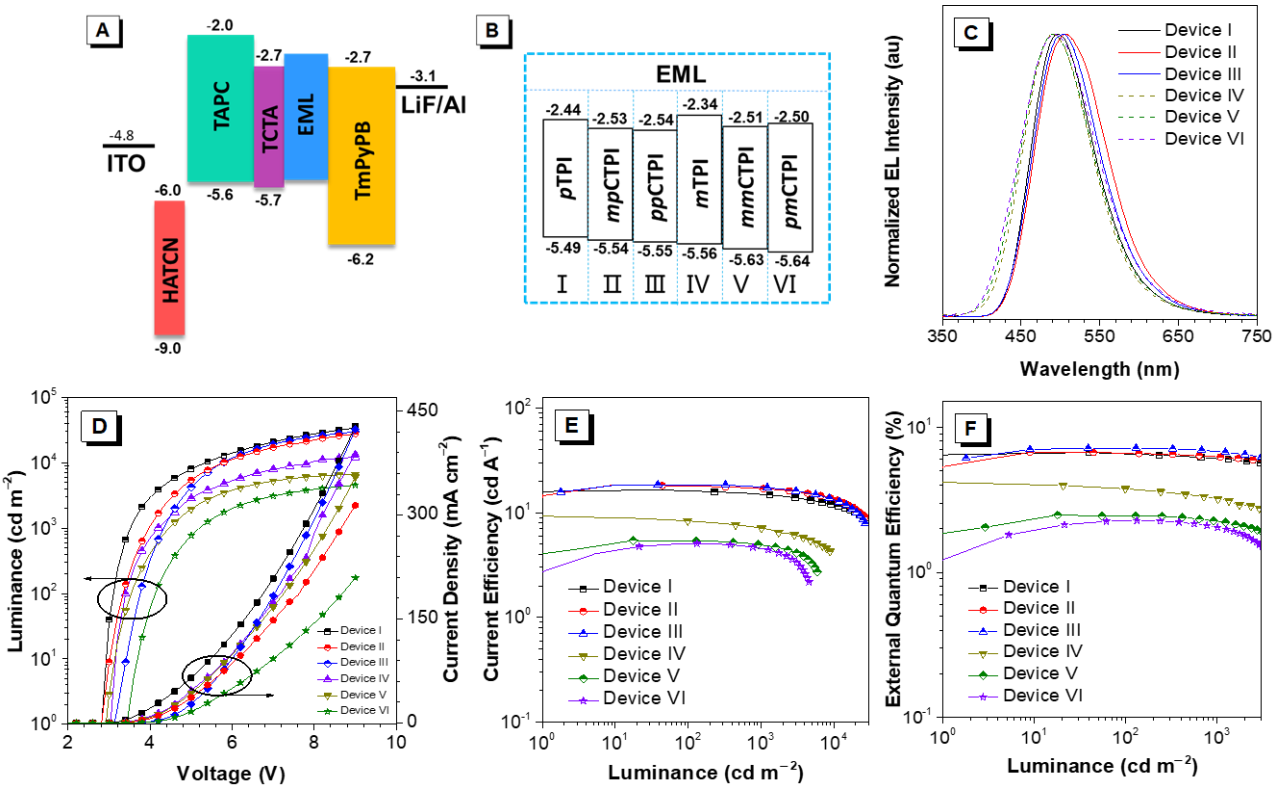

Fig. 9 (A) and (B) Energy level diagrams; (C) EL spectra at 10 mA cm^{-2}; (D) current density–voltage–luminance (*J*-*V*-*L*) characteristics; (E) current efficiency versus luminance curves; and (F) EQE versus luminance curves of the non-doped OLEDs based on the six AIEgens.

View Article Online DOI: 10.1039/C9TC01457F

where, η_{EL} is the EQE, η_{rec} is the electron-hole recombination proportion (assumed to be 100%), η_s is the EUE, η_{PL} is the PLQY of neat film, and η_{out} is the light out coupling efficiency (usually estimated from 20% to 30%, and calculated using 25% here).[22]

As shown in the EL spectra, the devices based on TPE *para*- and *meta*-linked compounds exhibited bluish green and sky-blue emissions, respectively, and their EL peaks are close to their PL peaks of neat films. All the devices exhibited low turn-on voltages (V_{on}) under 3.5 eV, thanks to the bipolar properties from PI unit.[23] And among them, the TPE *para*-linked compounds displayed lower V_{on} than *meta*-linked ones because of more balanced carrier transport stem from their larger molecular conjugation.[24] Enjoying the higher PLQYs, the former exhabited better EL performances than the latter. The EQE_{max} of *p*TPI, *mp*CTPI and *pp*CTPI were 6.32%, 6.71%, and 7.16%, respectively, much higher than those of *m*TPI (3.98%), *mm*CTPI (2.27%) and *pm*CTPI (2.48%). In addition, the cynao group had a very positive effect on increasing EUE. For *p*TPI and *m*TPI, the EUE values were calculated to be 28% and 33.4%, respectively, which had slightly exceeded the theoretical limit of spin statistics of fluorescent emitters. For the cyano-containing compounds, the EUE was increased obviously because of larger CT component in the HLCT states. When the cynao group was linked at the *para* position, the EUE reached excellent values of 48.1 % for *pp*CTPI and 48.4% for *pm*CTPI. The improvment in EUEs was consitent with the above analysis of more excitons conversion channels. Furthermore, taking the advantage of AIE property, low efficiency roll-off was also achieved in these non-doped OLEDs. The non-doped OLED based on *pp*CTPI exhibited maximum *L*, η_c, η_p and EQE of up to 31070 cd m^{-2}, 18.46 cd A^{-1}, 16.32 lm W^{-1} and 7.16 %, respectively. Notably, the deivce showed excellent efficiency stability as evidenced by a very small efficiency roll-off of 4.0 % at 1000 cd m^{-2}.

Conclusions

In order to enhance the PLQYs of HLCT-based compounds in aggregates and develop a feasible molecular design strategy for high-efficiency OLED emitters, by incorporating TPE units and cyano groups to C2 and N1 substitution with different patterns, six fluorescent PI derivatives were prepared. The systematic photophysical analysis in various formations showed that, the six compounds exhibited AIE characteristics with high PLQYs in aggregates, and had tunable excited state distribution of LE and CT components in HLCT states. Combining the photophysical and electrochemical measurements and theoretical calculations, the impacts of molecular conjugation patterns on the LE/CT distribution, luminous efficiency, and exciton conversion channel were revealed, based on which the contributions of the crossed axes (long axis and short axis) with a vertical conformation was proposed. The performances of non-doped OLEDs based on these PI derivatives proved our hypothesis. Amongst them compounds, *pp*CTPI exhibited the best EL performance with maximum *L*, η_c and η_p of up to 31070 cd m^{-2}, 18.46 cd A^{-1}, 16.32 lm W^{-1}, and the maximum EQE of 7.16 % with roll off of 4.0 % at 1000 cd m^{-2} luminance. These results demonstrated that, a strategy of reasonably superposing AIE unit to HLCT emitters via construcing a conformation of vertical cross axes is practically feasible in materials design.

Conflicts of interest

There are no conflicts to declare.

Acknowledgements

This work is financially supported by National Natural Science Foundation of China (21788102, 51673118 and 51603127), the Guangdong Natural Science Funds for Distinguished Young Scholar (2014A030306035), Science & Technology Program of Guangzhou (201804010218, 201804020027, 201704030069), the Innovation and Technology Commission of Hong Kong (ITC-CNERC14S01), and the Fundamental Research Funds for the Central Universities (2017JQ013).

Notes and references

1 (*a*) M. A. Baldo, M. E. Thompson, S. R. Forrest, *Nature*, 2000, **403**, 750; (*b*) A. C. Grimsdale, K. L. Chan, R. E. Martin, P. G. Jokisz, A. B. Holmes, *Chem. Rev.*, 2009, **109**, 897.

2 M. A. Baldo, D. F. O'Brien, M. E. Thompson, S. R. Forrest, *Phys. Rev. B*, 1999, **60**, 14422.

3 (*a*) H. Uoyama, K. Goushi, K. Shizu, H. Nakamura, C. Adachi, *Nature,* 2012, **492**, 234; (*b*) Y. Geng, A. D'Aleo, K. Inada, L.-S. Cui, J. U. Kim, H. Nakanotani, C. Adachi*, Angew. Chem. Int. Ed.*, 2017, **56**, 16536; (*c*) J. Guo, X.-L. Li, H. Nie, W. Luo, S. Gan, S. Hu, R. Hu, A. Qin, Z. Zhao, S.-J. Su, B. Z. Tang, *Adv. Funct. Mater.*, 2017, **27**, 1606458; (*d*) D. Zhang, X. Song, M. Cai, H. Kaji, L. Duan, *Adv. Mater.*, 2018, **30**, 1705406; (*e*) X. Chen, Z. Yang, Z. Xie, J. Zhao, Z. Yang, Y. Zhang, M. P. Aldred, Z. Chi, *Mater. Chem. Front.*, 2018, **2**, 1017.

4 (*a*) D. Yang, P. Duan, M. Liu, *Angew. Chem. Int. Ed.*, 2018, **57**, 9357; (*b*) J. Han, Y. Jiang, A. Obolda, P. Duan, F. Li, M. Liu, *J. Phys. Chem. Lett.,* 2017, **8**, 5865; (*c*) P. Duan, N. Yanai, Y. Kurashige, N. Kimizuka, *Angew. Chem. Int. Ed.*, 2015, **54**, 7544; (*d*) X. Tang, Q. Bai, T. Shan, J. Li, Y. Gao, F. Liu, H. Liu, Q. Peng, B. Yang, F. Li, P. Lu, *Adv. Funct. Mater.*, 2018, **28**, 1705813.

5 (*a*) W. Li, D. Liu, F. Shen, D. Ma, Z. Wang, T. Feng, Y. Xu, B. Yang, Y. Ma, *Adv. Funct. Mater.*, 2012, **22**, 2797; (*b*) R. K. Konidena, K. R. Justin Thomas, D. Kumar Dubey, S. Sahoo, J. H. Jou, *Chem. Commun.*, 2017, **53**, 11802; (*c*) Y. Gao, S. Zhang, Y. Pan, L. Yao, H. Liu, Y. Guo, Q. Gu, B. Yang, Y. Ma, *Phys. Chem. Chem. Phys.*, 2016, **18**, 24176; (*d*) C. Wang, X.-L. Li, Y. Gao, L. Wang, S. Zhang, L. Zhao, P. Lu, B. Yang, S.-J. Su, Y. Ma, *Adv. Opt. Mater.*, 2017, **5**, 1700441.

6 (*a*) B. Li, G. Tang, L. Zhou, D. Wu, J. Lan, L. Zhou, Z. Lu, J. You, *Adv. Funct. Mater.*, 2017, **27**, 1605245; (*b*) W. Z. Yuan, X. Bin, G. Chen, Z. He, J. Liu, H. Ma, Q. Peng, B. Wei, Y. Gong, Y. Lu, G. He, Y. Zhang, *Adv. Opt. Mater.*, 2017, **5**, 1700466; (*c*) S. Zhang, W. Li, L. Yao, Y. Pan, F. Shen, R. Xiao, B. Yang, Y. Ma, *Chem. Commun.*, 2013, **49**, 11302; (*d*) Y. Pan, W. Li, S. Zhang, L. Yao, C. Gu, H. Xu, B. Yang, Y. Ma, *Adv. Opt. Mater.*, 2014, **2**, 510.

7 (*a*) Y. Hong, J. W. Y. Lam, B. Z. Tang, *Chem. Soc. Rev.*, 2011, **40**, 5361; (*b*) J. Mei, N. Leung, R. Kwok, J. W. Y. Lam, B. Z. Tang, *Chem. Rev.*, 2015**, 115**, 11718; (*c*) Z. Zhao, B. He, B. Z. Tang, *Chem. Sci.*, 2015, **6**, 5347; (*d*) L. Pan, Y. Cai. H. Wu, F. Zhou, A. Qin, Z. Wang, B. Z. Tang, *Mater. Chem. Front.*, 2018, **2**, 1310.

8 (*a*) J. D. Luo, Z. L. Xie, J. W. Y. Lam, L. Cheng, H. Y. Chen, C. F. Qiu, H. S. Kwok, X. W. Zhan, Y. Q. Liu, D. B. Zhu, B. Z. Tang, *Chem. Commun.*, 2001, 1740; (*b*) H. Nie, K. Hu, Y. Cai, Q. Peng, Z. Zhao, R. Hu, S.-J. Su, J. Chen, A. Qin, B. Z. Tang, *Mater. Chem. Front.*, 2017, **1**, 1125; (*c*) Q. Li, Z. Li, *Adv. Sci.*, 2017, **4**, 1600484.

9 (*a*) Z. Zhao, J. W. Y. Lam, B. Z. Tang, *J. Mater. Chem.*, 2012, **22**, 23726; (*b*) J. Yang, J. Huang, Q. Q. Li, Z. Li, *J. Mater. Chem.C.*, 2016, **4**, 2663; (*c*) F. Song, Z. Xu, Q. Zhang, Z. Zhao, H. Zhang, W. Zhao, Z. Qiu, C. Qi, H. Zhang, H. H. Y. Sung, I. D. Williams, J. W. Y. Lam, Z. Zhao, A. Qin, D. Ma, B. Z. Tang, *Adv. Funct. Mater.,* 2018, **28**, 1800051; (*d*) J. Yang, L.Li, Y. Yu, Z. Ren, Q. Peng, S. Ye, Q. Li, Z. Li, *Mater. Chem. Front.*, 2017, **1**, 91-99; (*e*) Z. Li, *Sci. China Chem.*, 2017, **60**, 1107-1108.

10 (*a*) M. Y. Bian, Z. F. Zhao, Y. Li, Q. Li, Z. J. Chen, D. D. Zhang, S. F. Wang, Z. Q. Bian, Z. W. Liu, L. Duan, L. X. Xiao, *J. Mater. Chem.C.*, 2018, **6**, 745; (*b*) T. X. Liu, L. P. Zhu, C. Zhong, G. H. Xie, S. L. Gong, J. F. Fang, D. G. Ma, C. L. Yang, *Adv. Funct. Mater.*, 2017, **27**, 1606384; (*c*) T. C. Yu, L. L. Liu, Z. Q. Xie, Y. G. Ma, *Sci. China Chem.*, 2015, **58**, 907.

11 (*a*) Z. Wang, X. Li, K. Xue, H. Li, X. Zhang, Y. Liu, Z. Yu, P. Lu, P. Chen, *J. Mater. Chem.C.*, 2016, **4**, 1886; (*b*) Z. Wang, Y. Feng, S. Zhang, Y. Gao, Z. Gao, Y. Chen, X. Zhang, P. Lu, B. Yang, P. Chen, Y. Ma, S. Liu, *Phys. Chem. Chem. Phys.*, 2014, **16**, 20772; (*c*) S. Zhang, L. Yao, Q. Peng, W. Li, Y. Pan, R. Xiao, Y. Gao, C. Gu, Z. Wang, P. Lu, F. Li, S. Su, B. Yang, Y. Ma, *Adv. Funct. Mater.*, 2015, **25**, 1755.

12 (*a*)Z. Gao, K. Wang, F. Liu, C. Feng, X. He, J. Li, B. Yang, B. Zou, P. Lu, *Chem. Eur. J.*, 2017, 23, 773; (*b*) B. Xu, J. He, Y. Mu, Q. Zhu, S. Wu, Y. Wang, Y. Zhang, C. Jin, C. Lo, Z. Chi, A. Lien, S. Liu, J. Xu, *Chem. Sci.*, 2015, **6**, 3236.

13 Y. Yuan, J. Chen, F. Lu, Q. Tong, Q. Yang, H. Mo, T. Ng, F. Wong, Z. Guo, J. Ye, Z. Chen, X. Zhang, C. Lee, *Chem. Mater.*, 2013, **25**, 4957.

14 J. Yang, Q. X. Guo, J. Q. Wang, Z. C. Ren, J. X. Chen, Q. Peng, D. G. Ma, Z. Li, *Adv. Opt. Mater.*, 2018, **6**, 1800342.

15 (*a*) B. Chen, H. Zhang, W. Luo, H. Nie, R. Hu, A. Qin, Z. Zhao, B. Z. Tang, *J. Mater. Chem.C.*, **2017**, *5*, 960-968; (*b*) Y. Cai, C. Shi, H. Zhang, B. Chen, K. Samedov, M. Chen, Z. Wang, Z. Zhao, X. Gu, D. Ma, A. Qin, B. Z. Tang, *J. Mater. Chem.C.*, 2018, **6**, 6534; (*c*) Y. Cai, C. Gui, K. Samedov, H. F. Su, X. G. Gu, S. W. Li, W. W. Luo, H. H. Y. Sung, J. W. Y. Lam, R. T. K. Kwok, I. D. Williams, A. J. Qin, B. Z. Tang, *Chem. Sci.*, 2017, **8**, 7593.

16 (*a*) T. Nakagawa, S. Y. Ku, K. T. Wong, C. Adachi, *Chem. Commun.*, 2012, **48**, 9580; (*b*) J. Guo, X. L. Li, H. Nie, W. W. Luo, R. R. Hu, A. J. Qin, Z. J. Zhao, S. J. Su, B. Z. Tang, *Chem. Mater.*, 2017, **29**, 3623.

17 S. Tang, W. J. Li, F. Z. Shen, D. D. Liu, B. Yang, Y. G. Ma, *J. Mater. Chem.*, 2012, **22**, 4401.

18 (*a*) D. Hu, F. Shen, H. Liu, P. Lu, Y. Lv, D. Liu, Y. Ma, *Chem. Commun.*, 2012, **48**, 3015; (*b*) H. Liu, P. Chen, D. Hu, X. Tang, Y. Pan, H. Zhang, W. Zhang, X. Han, Q. Bai, P. Lu, Y. Ma, *Chem. Eur. J.*, 2014, **20**, 2149.

19 (*a*) S. K. Kim, B. Yang, Y. I. Park, Y. G. Ma, J. Y. Lee, H. J. Kim, J. Park, *Org. Electron.*, 2009, **10**, 822; (*b*) B. Yang, S. K. Kim, H. Xu, Y. I. Park, H. Y. Zhang, C. Gu, F. Z. Shen, C. L. Wang, D. D. Liu, X. D. Liu, M. Hanif, S. Tang, W. J. Li, F. Li, J. C. Shen, J. W. Park, Y. Ma, *Chemphyschem*, 2008, **9**, 2601.

20 Z. R. Grabowski, K. Rotkiewicz, W. Rettig, *Chem. Rev.*, 2003, **103**, 3899.

21 J. R. Sheats, H. Antoniadis, M. Hueschen, W. Leonard, J. Miller, R. Moon, D. Roitman, A. Stocking, *Science*, 1996, **273**, 884.

22 (*a*) M. Segal, M. Singh, K. Rivoir, S. Difley, T. V. Voorhis, M. A. Baldo, *Nat. Mater.*, 2007, **6**, 374; (*b*) S. Difley, D. Beljonne, T. V. Voorhis, *J. Am. Chem. Soc.*, 2008, **130**, 3420.

23 Z. Wang, P. Lu, S. Chen, Z. Gao, F. Shen, W. Zhang, Y. Xu, H. Kwok, Y. Ma, *J. Mater. Chem.*, 2011, **21**, 5451.

24 D. Dang, Z. Wang, K. Liu, Y. Liu, H. Sung, I. Willians, R. Kwok, J. W. Y. Lam, S.-J. Su, B. Z. Tang, *Adv. Electron. Mater.*, 2018, **4**, 1800354.

View Article Online
DOI: 10.1039/C9TC01453E

TOC

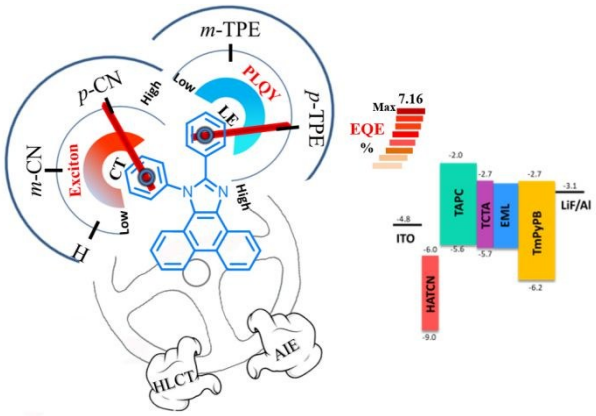

Combining HLCT and AIE characters, six phenanthroimidazole derivatives are